Sea Surface Height Estimation by Ground-Based BDS GEO Satellite Reflectometry

Jianming Wu, Yanling Chen, *Member, IEEE*, Fan Gao, Peng Guo, Xiaoya Wang, Xinliang Niu, Mengjie Wu, and Naifeng Fu

***Abstract*—Chinese BeiDou Navigation Satellite System (BDS) as a mixed constellation consists of not only medium earth orbit (MEO) satellites but also inclined geosynchronous orbit and geostationary earth orbit (GEO) satellites, of which the GEO satellites remain visible and stationary in the Asia–Pacific region almost all the time so as to better ensure the reflected signals stability and continuity, compared to using only MEO satellites in previous Global Navigation Satellite Systems Reflectometry remote sensing research. This article demonstrates ocean altimetry capability using reflected signals from BDS GEO satellite with coastal experiments conducted in Weihai, Shandong, China, on July 6 and July 9, 2019. By using only one GEO satellite, the precision of delay Doppler map and phase altimetry is up to decimeter (close to millimeter) level. And the results show that BDS GEO-R technique can be used to monitor small changes in ocean altimetry with high temporal resolution.**

***Index Terms*—Beidou Navigation Satellite System (BDS), delay Doppler map (DDM), Global Navigation Satellite Systems Reflectometry (GNSS-R), ocean altimetry, phase delay.**

I. Introduction

HUMAN activities such as shipping, ports, and fisheries are influenced by sea-level change, and sea-level rise is considered to be one of the consequences of global warming, and therefore, the measurement of its change is essential. Tide gauges have been commonly used for relative sea-level measurement [1]. However, this technique is affected by vertical movements of the ground such as glacial isostatic adjustment, coseismic and postseismic deformation, and land subsidence, which is corrected by Global Navigation Satellite Systems (GNSS) receivers later [2]. With the development of satellite technology, satellite radar altimetry technology has been applied to real-time monitoring of sea level. But in near-shore areas, satellite radar altimetry has poor precision due to the influence of the complex and volatile ocean environment. In 1993, Martín-Neira first proposed the Global Navigation Satellite Systems Reflectometry (GNSS-R) technology for ocean altimetry application [3]. And then, GNSS-R technology has attracted widespread attention for its low-cost, all-weather, and all-day global observation capabilities. In the following 20 years, many GNSS-R altimetry experiments were performed on the ground, airborne, and spaceborne platforms [4]–[9].

There are three ground-based GNSS-R methods to retrieve sea surface height (SSH): signal-to-noise ratio (SNR) method [10], [11], code delay method, and phase delay method [12], [13]. The SNR method altimetry setup contains only one GNSS receiver, which measures the surface height through the SNR evolution with the elevation angle of the GNSS satellite. The surface height can be also measured through the time delay between the direct and the reflected signal, which can be derived from both the ranging code (known as code delay or group delay) and the carrier phase (known as phase delay) of the received signals. The code/phase delay methods generally use two antennas to receive direct and reflected signals, respectively [14]. The precision of phase delay method reaches centimeter level [15]–[17], whereas limited by the chip length and the receiver chip resolution, the precision of code delay method only reaches meter level depending on the temporal resolution [18]–[21].

The current GNSS-R altimetry research mostly uses reflected signals from global positioning system (GPS) satellites constellation, which is composed of only medium earth orbit (MEO) satellites with relatively rapid speed and short visible time over the ground. By contrast, geostationary earth orbit (GEO) satellites in BeiDou Navigation Satellite System (BDS) are nearly stationary relative to the earth's surface. They can provide long-term stable specular point geometry and signal propagation paths for GNSS-R observations [22]. Recent studies have demonstrated the capability of sea surface altimetry using BDS-R altimetry technology with a limited amount of data [12], [23], [24]. However, the root-mean-square error (RMSE) between estimation results and measurements is decimeter level, still possible to be improved. And further GNSS-R SSH estimation research is needed to consolidate this concept and to understand its performance.

In order to verify the altimetry precision using one single BDS GEO satellite, we conducted experiments to receive the

Manuscript received May 23, 2020; revised July 28, 2020 and September 9, 2020; accepted September 11, 2020. Date of publication September 18, 2020; date of current version September 28, 2020. This work was supported in part by the National Key Research and Development Program of China under Grant 2016YFB0501405, in part by the National Natural Science Foundation of China project under Grants 41074019 and 11973073, and in part by the Natural Science Foundation of Shanghai under Grant 17ZR1435700. *(Corresponding authors: Yanling Chen; Peng Guo; Xiaoya Wang.)*

Jianming Wu is with the Shanghai Astronomical Observatory, Chinese Academy of Sciences, Shanghai 200030, China, and also with the University of Chinese Academy of Sciences, Beijing 100049, China (e-mail: wujm@shao.ac.cn).

Yanling Chen, Peng Guo, Xiaoya Wang, Mengjie Wu, and Naifeng Fu are with the Shanghai Astronomical Observatory, Chinese Academy of Sciences, Shanghai 200030, China (e-mail: ylchen@shao.ac.cn; gp@shao.ac.cn; wxy@shao.ac.cn; mjwu@shao.ac.cn; nffu@shao.ac.cn).

Fan Gao is with the Institute of Space Science, Shandong University, Weihai 264209, China (e-mail: gaofan@sdu.edu.cn).

Xinliang Niu is with the China Academy of Space Technology, Xi'an 710101, China (e-mail: xlniu1983@hotmail.com).

Digital Object Identifier 10.1109/JSTARS.2020.3024743

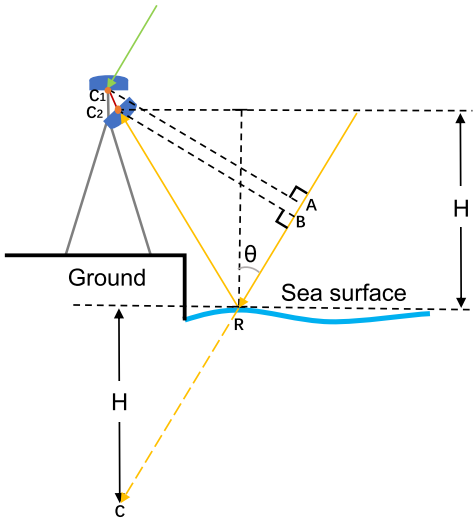

Fig. 1. Ground-based GNSS-R relative SSH estimation geometric relationship. H is the relative SSH. C_1 and C_2 are the phase centers of the RHCP and LHCP antennas. C is the mirror point of the LHCP antenna phase center. R is the specular point.

B1I reflected signals of BDS GEO satellite on July 6 and 9, 2019 (Beijing Time) in Weihai, Shandong Province, China. Our receiver is geared toward a wider range of applications. It not only outputs a pair of delay Doppler maps (DDMs) of direct and reflected signals every second but also outputs the in-phase and quadrature (I/Q) data of direct and reflected signals at a frequency of 1000 Hz. DDMs and I/Q data can be directly applied to sea state inversion. In this article, the relative SSH is derived by the code delay method using DDMs and the phase delay method using I/Q data. To further verify the influence of sea surface conditions on the relative SSH estimation by one BDS GEO satellite, we also conducted wind speed measurement.

The rest of this article is organized as follows. Section II introduces the GNSS-R relative SSH estimation method. Section III describes the experimental details, including the experimental site, equipment, data, and processing procedures. Section IV illustrates the relative SSH estimation results and further introduces a discussion. Finally, Section V concludes this article.

II. Methods

Fig. 1 presents the geometry of a typical coastal GNSS-R setup with the solid green line indicating the path of the direct signal and the solid yellow line for the reflected signal path. As the GNSS satellites are far away (e.g., >20 000 km for the GNSS MEO satellites and 36 000 km for the GNSS GEO satellites) from earth's surface, it can be assumed that the path of the direct signal and path of the incident signal are nearly parallel in this coastal setup.

H is the vertical distance from the sea surface to the left-hand circular polarization (LHCP) antenna, defined as relative SSH. θ is the incident angle. C_1 and C_2 are the phase centers of the right-hand circular polarization (RHCP) and LHCP antennas. R represents the specular point. The path difference between the direct signal and the reflected signal is defined as

$$D = AC = AB + BR + RC_2 \tag{1}$$

where AB is the projected length of $\boldsymbol{C_1C_2}$ on the path of the direct signal

$$AB = \boldsymbol{C_1C_2} \cdot \boldsymbol{e}_{AB}. \tag{2}$$

The relationship between the relative SSH and the path difference D can be obtained as

$$H = \frac{D - AB}{2\cos(\theta)}. \tag{3}$$

$\hat{D}$ is estimated through the delay difference between the direct and reflected signal. Similar to traditional GNSS positioning, $\hat{D}$ is affected by various factors, including the phase center errors of the antennas ε_{PC}, carrier phase wind-up ε_{PWU} [25], troposphere and ionospheric delay difference $\varepsilon_{\text{Trop}}$, $\varepsilon_{\text{Iono}}$ between reflected and direct signals, and observation noise ε, etc. $\hat{D}$ is expressed as

$$\hat{D} = AC + \varepsilon_{PC} + \varepsilon_{\text{PWU}} + \varepsilon_{\text{Trop}} + \varepsilon_{\text{Iono}} + \varepsilon. \tag{4}$$

For a GNSS receiver on the earth surface receiving forward scattering signals, it can be assumed that the ionospheric and tropospheric delay differences between the direct and reflected signals are identical. Therefore, when we estimate the path difference $\hat{D}$ between the direct and reflected signals, the delay differences in the troposphere and ionosphere can be eliminated. Related to the positions of transmitting antenna and receiving antenna, antenna phase center error ε_{PC} is composed of phase center variation ε_{PCV} and phase center offset ε_{PCO}

$$\varepsilon_{PC} = \varepsilon_{\text{PCV}} + \varepsilon_{\text{PCO}}. \tag{5}$$

The phase center offset ε_{PCO} is generally a fixed value and could be eliminated in relative SSH estimation. The phase center variation ε_{PCV} is usually within 1 cm not considered in this article. The phase wind-up error ε_{PWU} can be ignored because of hardly relative movement between GEO satellite and our ground-based receiver platform.

In this article, we apply two methods, i.e., code delay method and the phase delay method, to estimate the relative SSH. After that, once the absolute height of the ground is obtained by a certain method, for example, precise point positioning, we can calculate the absolute SSH. However, we only discuss the relative SSH in this article.

A. Code Delay Method

DDM is the fundamental observation for spaceborne GNSS-R. It represents the distribution of signal power in the reflector of the earth surface. Currently, DDM is used to retrieve sea surface wind speed, detect sea ice concentration and oil slick presence [26]–[29]. In 2000, Zavorotny and Voronovich [30] proposed the method for calculating DDM, which is expressed by the following formula after modification:

$$\left\langle |Y(\tau, f)|^2 \right\rangle = \frac{P_t G_t \lambda^2 T_i^2}{(4\pi)^3} \iint_A \frac{G_r \Lambda^2(\tau) S^2(f)}{{R_t}^2 {R_r}^2} \sigma^0 dA \tag{6}$$

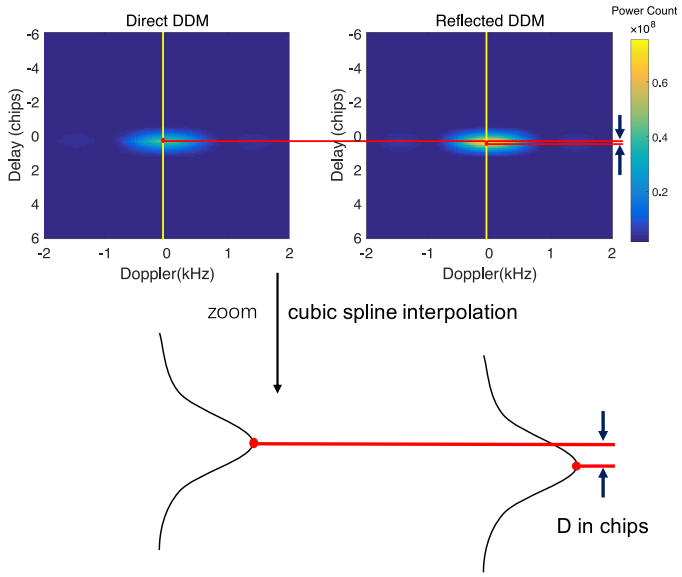

Fig. 2. Process of the code delay method to obtain D. The DDMs in this figure are derived from the measured data.

where $\left\langle |Y(\tau, f)|^2 \right\rangle$ is the power on the DDM at τ code delay and f Doppler shift, P_t and G_t are the transmitting power and gain of the GNSS transmitter antenna, λ is the wavelength of the GNSS electromagnetic wave, T_i is the coherent integration time, G_r is the gain of the receiver antenna, $\Lambda(\tau)$ is GNSS signal spreading function in delay, $S(f)$ is the frequency response of the GNSS signal, R_t and R_r are the distances from the sea surface scattering point (x, y) to the GNSS transmitter antenna and the GNSS-R receiver antenna, σ^0 is the sea surface scattering coefficient, and A is the integration area.

Analogous to positioning, the code delay can be obtained by calculating the peak offset between the direct and reflected DDMs. The code delay precision depends on the bandwidth of the signal. The bandwidth of BDS B1I code is 2.046 MHz, which is twice wider than GPS C/A code, implying a better range precision. In order to increase the ranging resolution, we use cubic spline interpolation to make the delay sampling rate change from 10 to 10 kHz.

Fig. 2 describes the process of the code delay method. First, we find the columns (the yellow line) where the maximums of direct DDM and reflected DDM are located. Then we use cubic spline interpolation for these two columns to increase their ranging resolution. Finally, we search for the code delays corresponding to the maximums of the two columns, calculate difference between the two code delays, and obtain the spatial path difference $\hat{D}$ between the direct and reflected signals to estimate the relative SSH by (3).

B. Phase Delay Method

Considering that the code delay method is limited by the bandwidth of the transmitted signal, we also use another phase delay method to estimate relative SSH. The scattered electromagnetic waves on the rough sea surface include the coherent and incoherent components. As sea surface roughness increases, the coherent components gradually decrease. Ocean waves, including wind waves and swell waves, will have an effect on the coherent components. When the coherent components of the reflected signal are strong enough, the carrier phase of the coherent components can be used to estimate the relative SSH.

In this experiment, the I/Q components of the direct and reflected signals are output by our GNSS-R receiver. In traditional GNSS receiver navigation data are demodulated from I/Q data. It is similar to the process of direct signals in our receiver. Once the receiver obtains the navigation data from the direct signals, it directly corrects I/Q data of the reflected signals to remove the navigation data. So that the output I/Q data of the receiver only retains the carrier.

According to [13], the coherent components phase used to estimate the relative SSH changes continuously in $[-\pi, \pi]$. Once the phases are distributed in the four quadrants of the complex plane continuously and uniformly, the coherent components are sufficient to estimate SSH. Because the relative position between the GEO satellite and the receiving antenna is almost constant and the signals have little Doppler shift. There is a strong coherence between the direct and reflected signals of BDS GEO satellites that brings great advantage for the relative SSH estimation. Furthermore, paper [31] explains that the wind and wave requirements to enable sufficient coherence appear to be below 6 m/s wind and 1.5 m SWH. Our experiments were conducted under this condition.

During the data processing, we first record H_0. It consists of the distance from LHCP antenna center to the ground and the distance from the ground to the water measured at the beginning epoch of the experiment. Then we pick out the direct and reflected signals I/Q data with continuous phase to calculate the phase differences between the direct and reflected signals. After eliminating the integer ambiguities of phase differences, we converted the phase differences to the range changes $\Delta\hat{D}$ using

$$\Delta\hat{D} = \frac{\lambda(\varphi_R - \varphi_D)}{2\pi} \tag{7}$$

where φ_D and φ_R are the phase of direct and reflected signals without the integer ambiguities.

According to (3), the changes of the relative SSH $\Delta\hat{H}$ are obtained from $\Delta\hat{D}$. Then, the relative SSH is obtained by

$$\hat{H} = H_0 + \Delta\hat{H}. \tag{8}$$

C. Assessment Method

In order to assess the bias and stability of the GNSS-R relative SSH estimation, we used three indicators: the mean bias $\overline{\delta}$, the standard deviation σ (Std), and the RMSE, which are demonstrated as

$$\overline{\delta} = \frac{1}{N}\sum_{i=1}^{N}(\hat{H}_i - H_i) = \frac{1}{N}\sum_{i=1}^{N}\delta_i \tag{9}$$

$$\sigma = \sqrt{\frac{1}{N}\sum\nolimits_{i=1}^{N}(\delta_i - \overline{\delta})^2} \tag{10}$$

$$\text{RMSE} = \sqrt{\frac{1}{N}\sum\nolimits_{i=1}^{N}\delta_i^2} \tag{11}$$

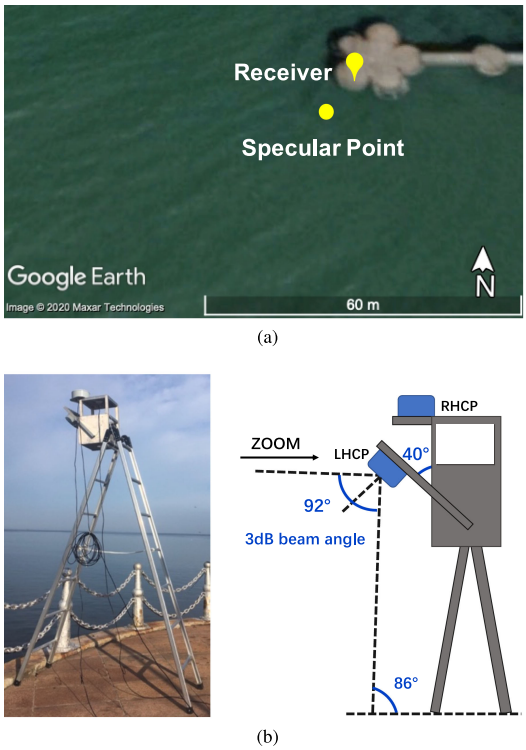

Fig. 3. Experimental site is on a trestle about 113 m away from the sea with wide vision and no interference. LHCP and RHCP antennas are erected with the height of about 4 m on the trestle bridge. The specular point is about 7 m away from the experimental site. (a) Satellite image of study area. (b) Experimental scene.

where H_i is defined as the measured relative SSH, and $\hat{H}_i$ is the estimated result of the GNSS-R method.

III. Case Study

A. Study Area

We carried out relative SSH retrieval experiments in Weihai, Shandong Province (122°2′44.93″ E, 37°32′2.75″ N), China. Weihai is located the east of the Shandong Peninsula, East China and with sea in the north, east, and south sides. Satellite image of study area and experimental scene are shown in Fig. 3(a) and (b). The experimental site is located at the end of a trestle upon the stable bedrock, about 113 m away from the land, where our equipment hardly receives the reflected signals from the land. RHCP and LHCP antennas are set on the bracket with the height of about 4.0 m from the ground. The RHCP antenna pointed to the zenith. And the depression angle of the LHCP antenna is about 40°, the 3-dB beam angle about 92°. The far-range line of sight will reach the point where is tangent to the surface of the earth. And the angle between the near-range line of sight and sea surface is about 86° [see Fig. 3(b)].

B. Instruments

GNSS-R equipment is composed of three parts: antennas, receiver and bracket. Antennas include RHCP antenna, LHCP antenna, and navigation antenna. The navigation antenna provides the positioning information. And the RHCP antenna and

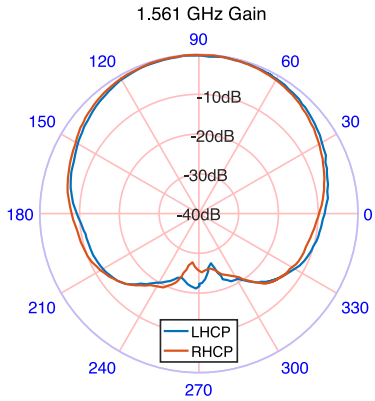

Fig. 4. RHCP and LHCP antennas pattern in elevation. In this polar coordinate system, the polar angle is the elevation angle and the polar radius is the magnitude of the gain. The blue line is the gain of the LHCP antenna and the orange line is the gain of the RHCP antenna. The 3-dB beam angle approximately is 92°.

TABLE I
Receiver Performance Parameters

Parameters	Value
Bandwidth (BDS B1)	1561.10 ± 20.46MHz
LNA gain	20 dB
Noise figure	1.8 dB
Sampling rate	25 Msps
Bit per sample	4 bits
Operating temperature	-40°C to +50°C
Power consumption	18 W
Weight	2 kg
Size	200×140×48 mm

LHCP antenna are exactly the same in structure, which receive the direct and reflected signals, respectively, by adjusting the different interfaces. The antenna gain is isotropic in the azimuth direction and anisotropic in the elevation direction (see Fig. 4). As the antenna is only a few meters above the sea surface, there could be direct signals received by the LHCP antenna as well. But LHCP antenna has a little gain (less than −30 dB) for direct signals (RHCP).

The RHCP, LHCP, and navigation antennas are connected to the receiver via radio frequency cables. The receiver is powered by 12 V dc power supply. When the signals are received by the antennas, the low-noise amplifier (LNA) in the receiver gains the signals again. The data are output to the SD card inserted in the receiver and also the computer by the network cable in real time. The receiver can receive GPS and BDS signals, and preferentially output the data with the highest SNR. Table I lists the receiver performance parameters.

In our study, the signals from BDS PRN 03 satellite showed the highest SNR. The output data consist of azimuth and elevation angle of this satellite, direct and reflected DDMs (see Fig. 2) using a 1-ms coherent integration time and 1000 times incoherent integration to reduce noise and I/Q data (see Fig. 5) without navigation information. DDM has a chip resolution of 0.1 chip and a Doppler resolution of 50 Hz, which are set when the receiver performs correlation calculations on both the delay and Doppler of the signals.

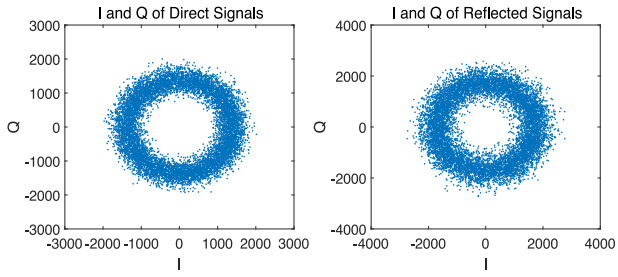

Fig. 5. Output data: I/Q distribution of direct and reflected signals.

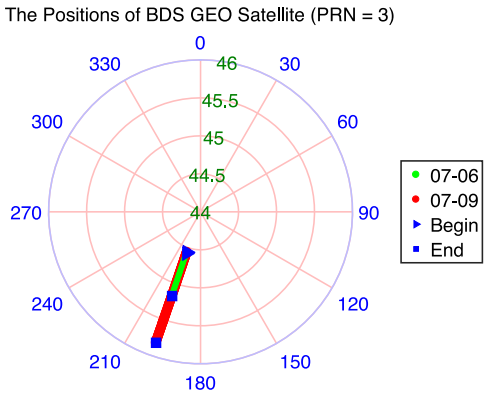

Fig. 6. Changes of the azimuth and elevation of the BDS GEO satellite (PRN 03) during the two experiments. The azimuth of the satellite was about 198.49° and nearly constant. Elevation angle changed about 1°.

Therefore the code delay resolution is 4.89 $\times 10^{-8}$ s and the ranging resolution is 14.65 m. The carrier frequency is 1561.098 MHz and the wavelength is about 19 cm. In addition to the GNSS-R data, a digital hot wire anemometer whose type is Smart Sensor AR866A was used to measure the wind speed. The anemometer is able to measure the wind speed in the range from 0 to 30 m/s with precision of 0.1 m/s at 1 Hz sampling rate.

C. Data

The first experiment output data spans from 6:51:56 to 10:10:17, about 3.5 h. The second experiment output data is from 6:35:04 to 11:41:37, about 5 h. The wind speed measurements are also collected with the anemometer during the GNSS-R data collections.

The main datasets used in our analysis include the following six parts.

1) The direct and reflected DDMs have dimensions of 121 × 81, corresponding to ±6 delay chips in 0.1 chip increments and a ±2 kHz Doppler frequency with 50 Hz intervals. Before the data are processed, we use the DDM SNR to remove abnormal data (for more detail, see Section III-D). Then, we use DDM to compute code delay.
2) Direct and reflected I/Q data: phase differences between the direct and reflected signals are extracted from the I/Q components of the correlation outputs.
3) The azimuth and elevation angles of the BDS GEO satellite PRN 03 are shown in Fig. 6.

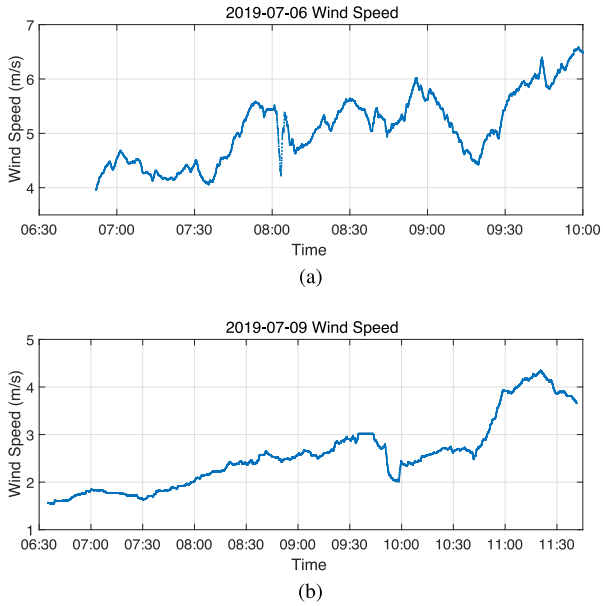

Fig. 7. Wind speed on July 6 and 9, 2019.

4) The relative SSH measurements are used as the reference data. They consist of the distances from the ground to sea surface measured every 15 min by a ruler and the heights of LHCP antenna center (the distance between LHCP antenna center and ground measured by a laser ranger). We choose quadratic polynomial to interpolate the measurements before the assessment.
5) The relative SSH estimation result data will go through a 30-min moving average.
6) Wind speed data (Fig. 7) are utilized to analyze possible error sources in relative SSH estimation. The wind speed measurement was subject to data missing due to the failure of anemometer and we filled these gaps with the nearest neighbor interpolation. In addition, a 500 s window moving average was employed to filter out high-frequency noise in wind speed data.

D. Data Quality Control

Sometimes our experiment was interfered by antenna shaking violently, an approaching small boat or poor cable connection, etc. The signal will thus get weak or even lost, and the thermal noise is flooding DDM. That appeared more frequently in the initial experiment on July 6. In order to remove abnormal DDMs, SNR method is adopted (different from the SNR method used for SSH estimation). The SNR is defined as

$$\mathrm{SNR} = 10 \lg \left(\frac{P - N}{N} \right). \tag{12}$$

P is the peak power average of 9 × 5 bins near the DDM center in the 121 × 81 size DDM. N is the average noise power from near signal-free 10 × 81 bins (the top 10 rows) of DDM shown in Fig. 2.

The SNR in two experiments is shown in Fig. 10. The reflected signals DDMs SNR threshold is set to 2 dB empirically. The directed signals DDMs SNR thresholds are set to 7 dB and −1 dB

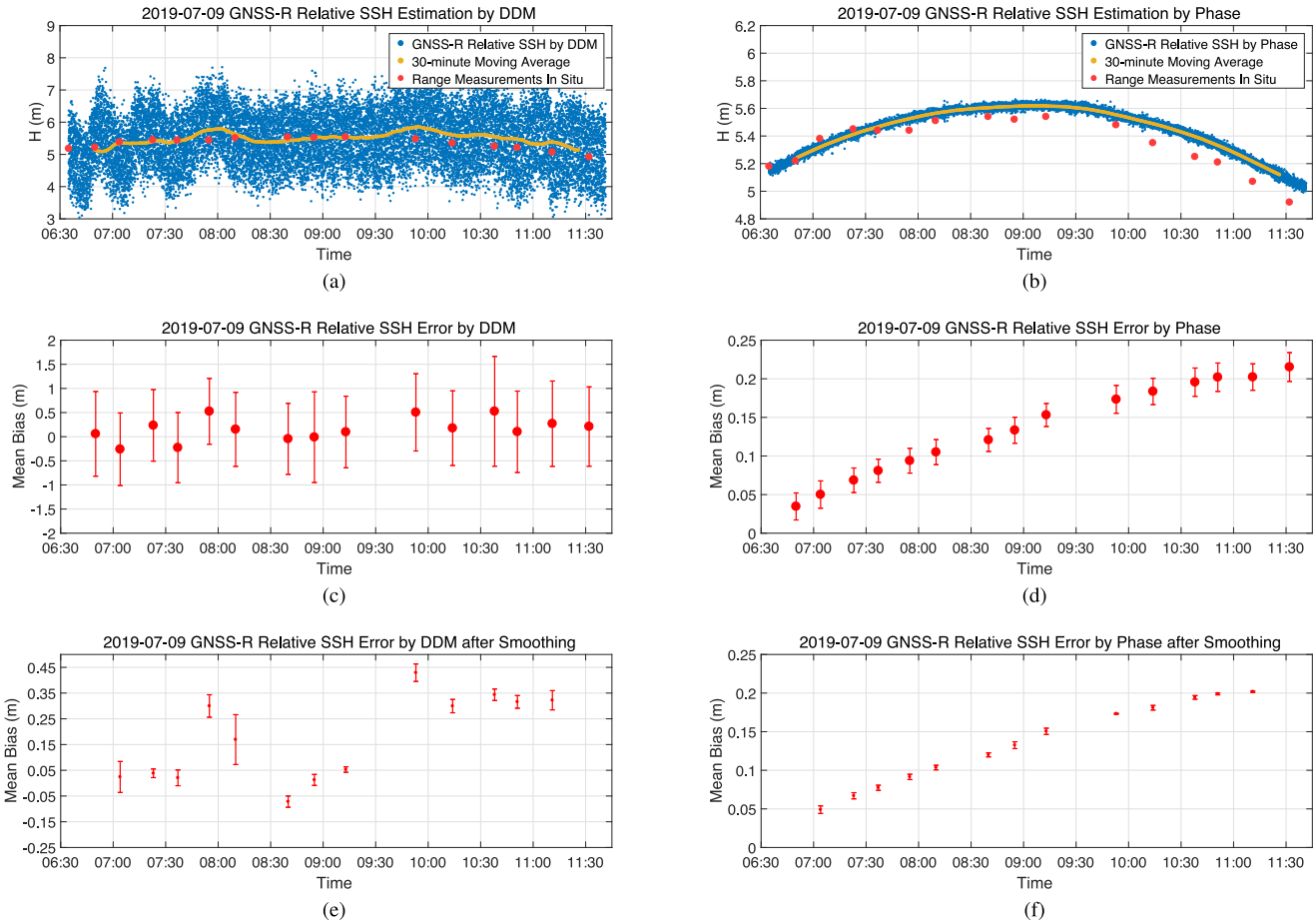

Fig. 8. Relative SSH by two methods on July 9, 2019. (a) and (b) Results of estimation. (c) and (d) Mean bias and standard deviation of estimation within 15 min before and after the measurement time. (e) and (f) Mean bias and standard deviation of estimation after smoothing within 15 min before and after the measurement time. (a), (c), and (e) are obtained by code delay method. (b), (d), and (f) are obtained by phase delay method.

for two experiments as reference only. When DDMs SNR is higher than the threshold, the DDM is considered normal. By using this criterion about 16% of the total data collected on July 6 is removed, and about 1% of the aggregate data on July 9 is discarded. On July 6 after about 9:40, the antenna shook violently and could not point to the sea stably. As a result, the reflected signals DDMs SNR is close to -40 dB (not shown in Fig. 10). All the data after 9:40 are discarded.

IV. Results and Discussion

A. July 6, 2019 Acquisitions

The relative SSH results were derived by the GNSS-R data from 6:51 to 9:39. The experiment verified the feasibility of the relative SSH estimation by the two methods. Fig. 9 shows the first relative SSH results, and the two columns are the results of the code delay method and the phase delay method, where (a) and (b) the blue and red points are the relative SSH estimation results and measurements and the yellow line is a 30-min moving average of the estimation results.

From Fig. 9(a) and (b), we can find that the relative SSH has a declining trend of about 1 m, and the relative SSH estimations by code delay method fluctuate greatly compared with estimations by phase difference. The assessment results of the two methods are shown in Table II. Moving average improves standard deviation for both methods. The improvement of the mean bias of the code delay method is also more significant. As a result, RMSE of the code delay method is improved from meter level to decimeter level. The RMSE of phase method is stable at the centimeter level but slightly improved after smoothing.

TABLE II
Mean Bias, Standard Deviation, and RMSE of Relative SSH Estimation on July 6 With 4–6 m/s Wind Speed

Method	Mean Bias (cm)	Std (cm)	RMSE (cm)
Code	17.16	129.49	137.16
Code after smoothing	2.02	11.84	18.18
Phase	0.24	3.80	4.36
Phase after smoothing	-0.63	2.63	3.13

To analyze the mean biases and standard deviations change over time of the two methods, we drew Fig. 9(c)–(f), where each statistic is calculated within 15 min taking the red points in Fig. 9(a) or (b) as the midpoint. For the code delay method, the standard deviations fluctuate around 150 cm and up to 200 cm. After smoothing the mean biases reach centimeter level and the standard deviations are close to centimeter level. For phase method, the absolute values of mean biases are generally less

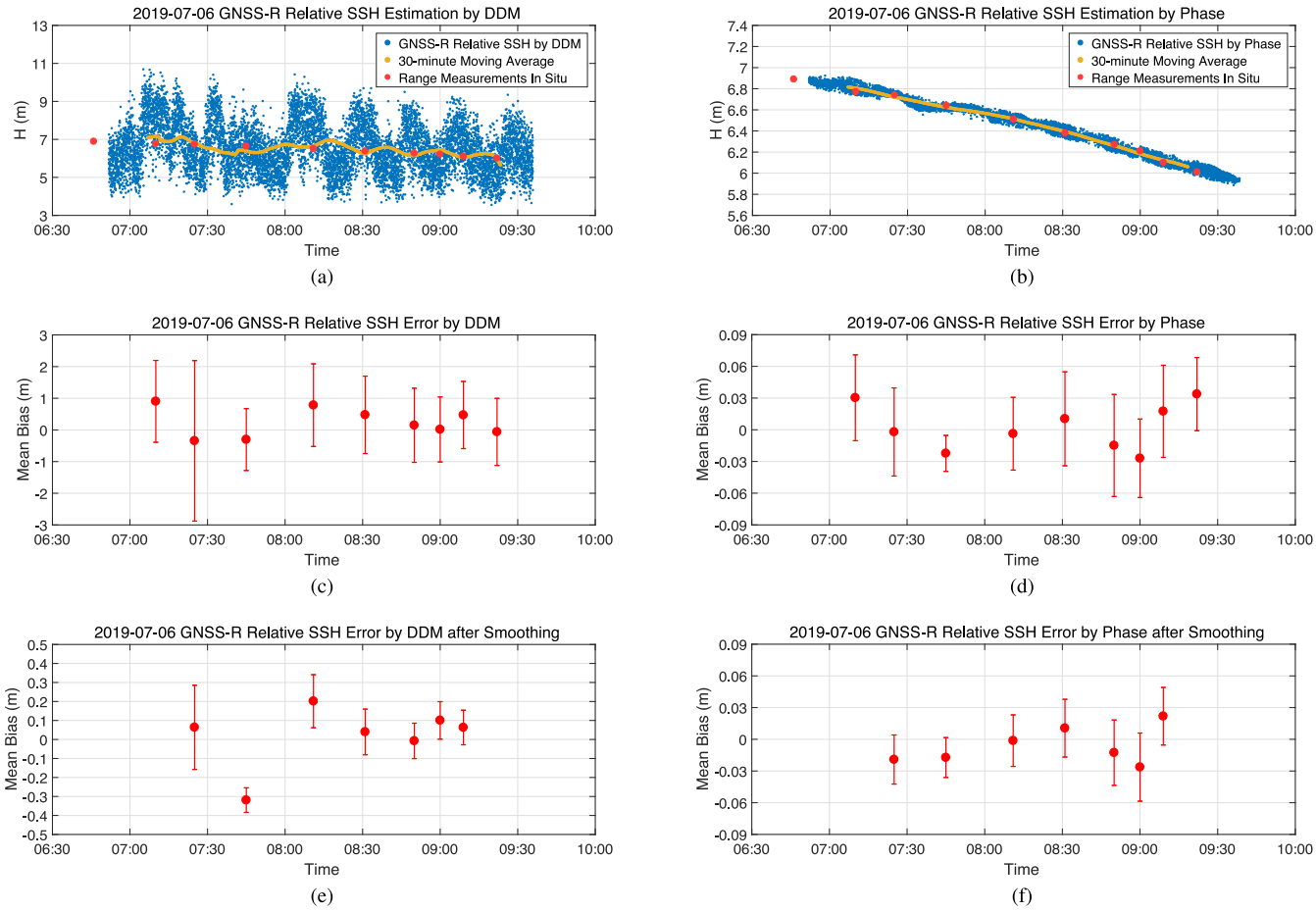

Fig. 9. Relative SSH by two methods on July 6, 2019. (a) and (b) Results of estimation. (c) and (d) Mean bias and standard deviation of estimation within 15 min before and after the observation time. (e) and (f) Mean bias and standard deviation of estimation after smoothing within 15 min before and after the observation time. (a), (c), and (e) are obtained by code delay method. (b), (d), and (f) are obtained by phase delay method.

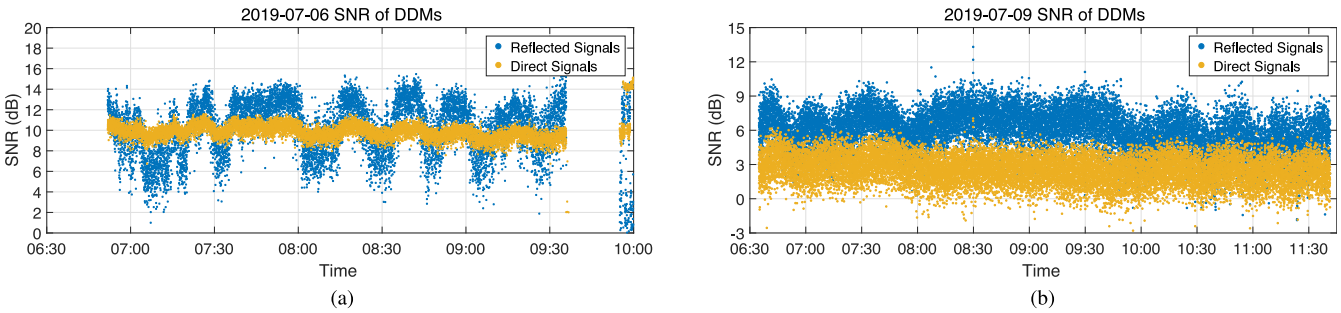

Fig. 10. SNR of DDMs in the two experiments. On July 6 after about 9:40, the antenna shaking violently and cannot point to the sea stably. In consequence, the reflected signals DDMs SNR is close to −40 dB (not shown in this figure). All the data after 9:40 are discarded.

than 3 cm and the standard deviations fluctuate around 3 cm. After smoothing the mean biases lightly increase at certain times and the standard deviations decrease by about a half.

Fig. 7(a) shows the wind speed measurement. It is found that the change of wind speed may affect the relative SSH estimation: the wind speed decreased slightly from about 7:00 to 7:30, when the mean bias decreased slightly as well; and from about 7:30 to 8:30 there was an upward trend in the wind speed and also the mean bias; after 8:50 the wind speed first decreased and then increased, and so did the mean bias. In addition to the possible influence of wind speed on the estimation, the residual errors described by (4) and (5) can also brought errors to the SSH estimation.

B. *July 9, 2019 Acquisitions*

The relative SSH results of the second experiment are shown in Fig. 8(a) and (b) and Table III. The meanings of point colors

TABLE III
MEAN BIAS, STANDARD DEVIATION, AND RMSE OF RELATIVE SSH ESTIMATION ON JULY 9 WITH 1–4 M/S WIND SPEED

Method	Mean Bias (cm)	Std (cm)	RMSE (cm)
Code	9.42	81.49	85.19
Code after smoothing	11.35	3.43	16.56
Phase	7.41	1.68	8.21
Phase after smoothing	7.39	0.29	7.58

are the same as these in Fig. 9. We can see from about 6:35 to 9:00 the relative SSH gradually increased with low tide. After about 9:00, the sea water rose and the relative SSH decreased.

Fig. 8(c)–(f) shows the variation of the mean bias and standard deviation of two methods. The standard deviations of code delay method fluctuate around 100 cm, compared with only about 1.5 cm of the phase method. After smoothing, the improvement of standard deviations is noticeable. The standard deviations are improved to centimeter level for code delay method and millimeter level for phase method. For the mean biases, moving average has little effect on the two methods, and there are upward trends with the magnitude of about 25 cm for the mean bias of phase method in Fig. 8(d) and (f).

The wind speed measured is shown in Fig. 7(b). It can be seen that the wind speed shows an increasing tendency during the data collection. But around 9:45 and 10:45, the wind speed suddenly decreased. And in Fig. 8(d), the rising tendency of the mean bias slightly stops around 9:45 and 10:45. It indicates that the change of wind speed may have a bearing on the SSH estimation. Further research is needed by subsequent experiments.

Due to the 24 h of orbital periodicity of the BDS GEO satellite, the satellite position changes of two experiments are similar, and we ignore the error caused by the relative position change of the GNSS satellite and the receiver.

C. Discussion

Tables II and III summarize that the standard deviation by phase delay method is better than the code delay method, and with no matter which method the standard deviation of the SSH estimation on July 9 with the wind speed between about 1 and 4 m/s is significantly better than that on July 6 with relatively larger wind speed. We can thus infer that relatively high wind speed and large waves may worsen the relative SSH estimation. Because the effects of electromagnetic bias will increase with the wind and waves [32]. And the waves will also reduce the coherent reflected signals [21].

Once the relative SSH estimation is smoothed, the standard deviations of both the code delay method and the phase delay method estimation can be further improved. In particular, a 30-min moving average can also weaken the large fluctuation in the code delay method. Compared with Fig. 10, there is a slight negative correlation between this fluctuation and reflected signals DDMs SNR. The fluctuation may be caused by the direct signals received by the LCHP antenna and is related to the code noise. But such a fluctuation of no more than 14.65 m (0.1 chip) is acceptable. And in result of the moving average the standard deviation of code delay method estimation decreased from 129.49 to 11.84 cm on July 6, and from 81.49 to 3.43 cm (centimeter level) on July 9, which is similar to the estimation by phase delay method using several MEO satellites. So we believe that the moving average is significantly necessary for the experiment.

However, the mean bias of relative SSH between GNSS-R estimation results and measurements on July 9 is larger than that on July 6 for the phase method. That has a more significant impact on the RMSE of phase delay method. In general, there are errors caused by changes in the relative position of the BDS GEO satellite and receiver, including $\varepsilon_{\mathrm{PCO}}$, $\varepsilon_{\mathrm{PCV}}$, and $\varepsilon_{\mathrm{PWU}}$. In Fig. 6, the azimuth of the BDS GEO satellite was almost unchanged, but the elevation angle changed about 1°. Due to the 24-h orbital periodicity of the BDS GEO satellite, the changes on two days are similar. The errors caused by the change in the elevation angle may be the reason for the increase of the mean bias in the phase method experiment on July 9.

V. CONCLUSION

Our two experiments on July 6 and 9, 2019 in Weihai, Shandong, China, indicate that one BDS GEO satellite can be efficiently utilized for continuous observation of GNSS-R and the relative SSH estimation with high precision as several MEO satellites.

In altimetry retrieval research by DDM group delay, the cubic spline interpolation was used to increase the resolution of the DDM. Compared with the relative SSH measurements, the standard deviation of code delay method has reached decimeter level. The best standard deviation is 81.49 cm at low wind speed (1–4 m/s). However, there is the fluctuation that has a slightly negative correlation with reflected signals DDMs SNR, which may be caused by the direct signals received by the LHCP antenna. After moving average of 30 min, the standard deviation has been significantly improved to centimeter level and the RMSE of code delay method also decreased from about 1 m to below 20 cm.

The altimetry stability of the phase delay method is obviously better than that by code delay method. Under the 4–6 m/s wind speed condition the standard deviation of altimetry reaches centimeter level (less than 4 cm). Under the condition of 1–4 m/s wind speed the standard deviation of altimetry is better than 2 cm; after moving average of 30 min, the standard deviation of phase delay method can achieve a millimeter level. However, RMSE only reached about 8 cm affected by the bias, which, according to our analysis, may be related to the electromagnetic bias caused by wind. Therefore, the bias needs further elimination. And meanwhile, the elevation angle of the BDS GEO satellite could have a relationship with antenna phase errors, which needs further investigation as well.

Our next work is to establish a long-term GNSS-R joint observatory for SSH, SWH, and meteorology to further refine the error models of GNSS-R SSH estimation, especially the error caused by antenna phase errors and electromagnetic bias. At the same time, we will improve SSH estimation by smooth pseudodistance of the carrier phase and dual-frequency GNSS-R

observation. Some communication and broadcast satellites are GEO satellites. We will also try to use these satellites for shore-based reflected signal altimetry in the future [33], [34]. In addition, GNSS-R tsunami monitoring technology based on SSH changes can be further developed through the long-term stable characteristics of GEO BDS-R observation area [35].

ACKNOWLEDGMENT

The authors are grateful to Y. He, W. Meng, and W. Yang, Shandong University, Weihai, China, for their help with the experiment.

REFERENCES

[1] T. Schöne, N. Schön, and D. Thaller, "IGS tide gauge benchmark monitoring pilot project (TIGA): Scientific benefits," *J. Geodesy*, vol. 83, no. 3, pp. 249–261, 2009.
[2] K. M. Larson, J. Lofgren, and R. Haas, "Coastal sea level measurements using a single geodetic GPS receiver," *Adv. Space Res.*, vol. 51, no. 8, pp. 1301–1310, 2013.
[3] M. Martín-Neira, "A passive reflectometry and interferometry system (PARIS): Application to ocean altimetry," *ESA J.*, vol. 17, no. 4, pp. 331–355, 1993.
[4] F. Soulat, M. Caparrini, O. Germain, P. Lopez-Dekker, M. Taani, and G. Ruffini, "Sea state monitoring using coastal GNSS-R," *Geophys. Res. Lett.*, vol. 31, no. 21, pp. 133–147, 2004.
[5] G. Ruffini and F. Soulat, "A GNSS-R geophysical model function: Machine learning for wind speed retrievals," *Cornell Univ. Library*, Ithaca, NY, USA, 2004, doi: 10.1109/LGRS.2019.2948566.
[6] M. P. Clarizia, C. P. Gommenginger, S. T. Gleason, M. A. Srokosz, M. D. Galdi, and C. Bisceglie, "Analysis of GNSS-R delay-Doppler maps from the UK-DMC satellite over the ocean," *Geophys. Res. Lett.*, vol. 36, no. 2, 2009, Art. no. L02608.
[7] J. Mashburn, P. Axelrad, C. Zuffada, E. Loria, A. O'Brien, and B. Haines, "Improved GNSS-R ocean surface altimetry with CYGNSS in the seas of Indonesia," *IEEE Trans. Geosci. Remote Sens.*, vol. 58, no. 9, pp. 6071–6087, Sep. 2020.
[8] E. Cardellach *et al.*, "Consolidating the precision of interferometric GNSS-R ocean altimetry using airborne experimental data," *IEEE Trans. Geosci. Remote Sens.*, vol. 52, no. 8, pp. 4992–5004, Aug. 2014.
[9] S. T. Lowe, C. Zuffada, Y. Chao, P. Kroger, L. Young, and J. L. Labrecque, "5-cm-precision aircraft ocean altimetry using GPS reflections," *Geophys. Res. Lett.*, vol. 29, no. 10, pp. 13-1–13-4, 2002.
[10] N. Roussel *et al.*, "Sea level monitoring and sea state estimate using a single geodetic receiver," *Remote Sens. Environ.*, vol. 171, no. 171, pp. 261–277, 2015.
[11] N. Wang, T. Xu, F. Gao, and G. Xu, "Sea level estimation based on GNSS dual-frequency carrier phase linear combinations and SNR," *Remote Sens.*, vol. 10, no. 3, p. 470, 2018.
[12] Y. Zhang, L. Tian, W. Meng, Q. Gu, Y. Han, and Z. Hong, "Feasibility of code-level altimetry using coastal BeiDou reflection (BeiDou-R) setups," *IEEE J. Sel. Topics Appl. Earth Observ. Remote Sens.*, vol. 8, no. 8, pp. 4130–4140, Aug. 2015.
[13] M. Martín-Neira, P. Colmenarejo, G. Ruffini, and C. Serra, "Altimetry precision of 1 cm over a pond using the wide-lane carrier phase of GPS reflected signals," *Can. J. Remote Sens.*, vol. 28, no. 3, pp. 394–403, 2002.
[14] J. Löfgren and R. Haas, "Sea level measurements using multi-frequency GPS and GLONASS observations," *EURASIP J. Adv. Signal Process.*, vol. 2014, no. 1, 2014, Art. no. 50.
[15] F. Fabra *et al.*, "Phase altimetry with dual polarization GNSS-R over sea ice," *IEEE Trans. Geosci. Remote Sens.*, vol. 50, no. 6, pp. 2112–2121, Jun. 2012.
[16] W. Li, E. Cardellach, F. Fabra, A. Rius, S. Ribo, and M. Martín-Neira, "First spaceborne phase altimetry over sea ice using TechDemoSat-1 GNSS-R signals," *Geophys. Res. Lett.*, vol. 44, no. 16, pp. 8369–8376, 2017.
[17] W. Li, E. Cardellach, F. Fabra, S. Ribó, and A. Rius, "Lake level and surface topography measured with spaceborne GNSS-Reflectometry from CYGNSS mission: Example for the lake Qinghai," *Geophys. Res. Lett.*, vol. 45, no. 24, pp. 13332–13341, 2018.
[18] W. Li, A. Rius, F. Fabra, E. Cardellach, S. Ribó, and M. Martín-Neira, "Revisiting the GNSS-R waveform statistics and its impact on altimetric retrievals," *IEEE Trans. Geosci. Remote Sens.*, vol. 56, no. 5, pp. 2854–2871, May 2018.
[19] W. Li, E. Cardellach, F. Fabra, S. Ribó, and A. Rius, "Assessment of spaceborne GNSS-R ocean altimetry performance using CYGNSS mission raw data," *IEEE Trans. Geosci. Remote Sens.*, vol. 58, no. 1, pp. 238–250, Jan. 2020.
[20] F. Fabra *et al.*, "Is accurate synoptic altimetry achievable by means of interferometric GNSS-R?," *Remote Sens.*, vol. 11, no. 5, p. 505, 2019.
[21] W. Liu *et al.*, "Coastal sea-level measurements based on GNSS-R phase altimetry: A case study at the Onsala Space Observatory, Sweden," *IEEE Trans. Geosci. Remote Sens.*, vol. 55, no. 10, pp. 5625–5636, Oct. 2017.
[22] W. Li *et al.*, "Initial results of typhoon wind speed observation using coastal GNSS-R of BeiDou GEO satellite," *IEEE J. Sel. Topics Appl. Earth Observ. Remote Sens.*, vol. 9, no. 10, pp. 4720–4729, Oct. 2016.
[23] Y. Zhang, B. Li, L. Tian, Q. Gu, Y. Han, and Z. Hong, "Phase altimetry using reflected signals from BeiDou GEO satellites," *IEEE Geosci. Remote Sens. Lett.*, vol. 13, no. 10, pp. 1410–1414, Oct. 2016.
[24] S. Jin, X. Qian, and X. Wu, "Sea level change from BeiDou Navigation Satellite System-Reflectometry (BDS-R): First results and evaluation," *Global Planet. Change*, vol. 149, pp. 20–25, 2017.
[25] G. Beyerle, "Carrier phase wind-up in GPS reflectometry," *GPS Solutions*, vol. 13, no. 3, pp. 191–198, 2009.
[26] N. Rodriguez-Alvarez, D. M. Akos, V. U. Zavorotny, J. A. Smith, A. Camps, and C. W. Fairall, "Airborne GNSS-R wind retrievals using delay," *IEEE Trans. Geosci. Remote Sens.*, vol. 51, no. 1, pp. 626–641, Jan. 2013.
[27] Q. Yan and W. Huang, "Sea ice sensing from GNSS-R data using convolutional neural networks," *IEEE Geosci. Remote Sens. Lett.*, vol. 15, no. 10, pp. 1510–1514, Oct. 2018.
[28] E. Valencia, A. Camps, N. Rodriguezalvarez, H. Park, and I. Ramosperez, "Using GNSS-R imaging of the ocean surface for oil slick detection," *IEEE J. Sel. Topics Appl. Earth Observ. Remote Sens.*, vol. 6, no. 1, pp. 217–223, Feb. 2013.
[29] Q. Yan and W. Huang, "Detecting sea ice from TechDemoSat-1 data using support vector machines with feature selection," *IEEE J. Sel. Topics Appl. Earth Observ. Remote Sens.*, vol. 12, no. 5, pp. 1409–1416, May 2019.
[30] V. U. Zavorotny and A. G. Voronovich, "Scattering of GPS signals from the ocean with wind remote sensing application," *IEEE Trans. Geosci. Remote Sens.*, vol. 38, no. 2, pp. 951–964, Mar. 2000.
[31] E. Cardellach *et al.*, "First precise spaceborne sea surface altimetry with GNSS reflected signals," *IEEE J. Sel. Topics Appl. Earth Observ. Remote Sens.*, vol. 13, pp. 102–112, Dec. 2019.
[32] A. Ghavidel, D. Schiavulli, and A. Camps, "Numerical computation of the electromagnetic bias in GNSS-R altimetry," *IEEE Trans. Geosci. Remote Sens.*, vol. 54, no. 1, pp. 489–498, Jan. 2016.
[33] S. C. Ho *et al.*, "Wideband ocean altimetry using Ku-Band and K-Band satellite signals of opportunity: Proof of concept," *IEEE Geosci. Remote Sens. Lett.*, vol. 16, no. 7, pp. 1012–1016, Jul. 2019.
[34] R. Shah and J. L. Garrison, "Precision of Ku-Band reflected signals of opportunity altimetry," *IEEE Geosci. Remote Sens. Lett.*, vol. 14, no. 10, pp. 1840–1844, Oct. 2017.
[35] Q. Yan and W. Huang, "Tsunami detection and parameter estimation from GNSS-R delay-Doppler map," *IEEE J. Sel. Topics Appl. Earth Observ. Remote Sens.*, vol. 9, no. 10, pp. 4650–4659, Oct. 2016.

Jianming Wu received the B.S. degree in geophysics from Chang'an University, Xi'an, China, in 2017. He is currently working toward the Ph.D. degree in remote sensing with Global Navigation Satellite Systems-Reflectometry and signal processing methods with the University of Chinese Academy of Sciences, Beijing, China.

Yanling Chen (Member, IEEE) was born in Henan, China, in 1980. She received the B.E. degree in surveying and mapping engineering from Tongji University, Shanghai, China, in 2002, and the Ph.D. degree in astrogeodynamics from Shanghai Astronomical Observatory, Chinese Academy of Sciences (CAS), Shanghai, China, in 2007.

From 2006 to 2007, she was a Research Assistant with The Hong Kong Polytechnic University. From 2007 to 2010, she was an Assistant Professor with the Shanghai Astronomical Observatory, CAS, where since 2010, she has been an Associate Professor. She is the author of more than 30 journal papers and conference presentation. She works at space-geodetic data processing and their applications using GNSS and SAR/InSAR space technologies. Her research interests include SAR/InSAR theory and applications on land surface deformation monitoring and sea surface wind retrieval, and GNSS/GNSS-R data processing and its remote sensing applications on sea surface wind, sea surface height, significant wave height, etc.

Dr. Chen has been a member of IEEE and Chinese Electronics Society since 2019.

Fan Gao received the B.E. degree in surveying and mapping engineering from Shandong University of Technology, Zibo, China, in 2010, and the Ph.D. degree in geodesy and surveying engineering from the University of Chinese Academy of Sciences, Beijing, China, in 2016.

From 2016 to 2018, he was a Postdoctoral Researcher with Shandong University, Weihai, China. Since 2018, he has been a Lecturer with the School of Space Science and Physics, Shandong University. His research interests include GNSS-R altimetry, GNSS software-defined receiver, satellite constellation design, and precise orbit determination.

Peng Guo was born in Zhejiang Province, China, in 1976. He received the Ph.D. degree in astrometry and celestial mechanics from the Shanghai Astronomical Observatory, Chinese Academy of Sciences, Shanghai, China, in 2006.

He is currently a Researcher and Doctoral Supervisor with the Shanghai Astronomical Observatory, Chinese Academy of Sciences. He has authored/coauthored more than 50 papers. His research interests include GNSS/LEO occultation technology and application research, ionospheric monitoring and modeling, and GNSS navigation and application.

Xiaoya Wang received the B.Sc. degree in astrometry from Nanjing University, Nanjing, China, in 1992, and the M.Sc. degree in GPS meteorology and Ph.D. degree in GNSS applications on geophysics from the Shanghai Astronomical Observatory, Chinese Academy of Sciences (CAS), Shanghai, China, in 1998 and 2001, respectively.

From 1992 to 1995, she was a Research Assistant with the Shanxi Astronomical Observatory, CAS. From 2002 to 2004, she was a Research Associate with The Hong Kong Polytechnic University. From 2005 to 2010, she was an Associate Professor with the Shanghai Astronomical Observatory, CAS, where since 2010, she has been a Professor. She visited DGFI for half year as a Visiting Professor, in 2012. She works at space-geodetic data processing and their applications. Her main research fields are GNSS data processing and its applications including precise orbit determination of satellites, GPS meteorology, crustal deformation monitoring, ionosphere monitoring, etc.

Prof. Wang has been a member of IAG JWG1.3 Intratechnique and Intertechnique Atmospheric Ties since 2015, and a member of IAU several Divisions since 2012.

Xinliang Niu received the B.E. degree in electronics and information engineering, in 2005 and the Doctorate degree in electronics science and technology from Xidian University, Xi'an, China, in 2010.

He is a Senior Engineer with the China Academy of Space Technology, Xi'an, China. He specializes in satellite navigation and remote sensing. He is the PI of ground verification subsystem of BuFeng-1 mission. Moreover, he also participated in R&D activities of Beidou Navigation Satellite System, Chang'e moon exploration satellite mission, etc.

Mengjie Wu was born in Henan Province, China, in 1992. She received the B.E. degree in geomatics engineering from Chang'an University, Xi'an, China, in 2012, and the Ph.D. degree in astrometry and celestial mechanics from Shanghai Astronomical Observatory, Chinese Academy of Sciences (CAS), Shanghai, China, in 2018.

From 2016 to 2017, she was a Visiting Scholar with the COSMIC Program Office, University Corporation for Atmospheric Research, Boulder, CO, USA. Since 2018, she has been an Assistant Professor with the Shanghai Astronomical Observatory, CAS. She is the author of ten articles. Her current research focuses on the development of global ionospheric model using spaceborne and ground-based observations, improving data processing techniques of radio occultation, topside and upper ionosphere, and plasmasphere modeling.

Naifeng Fu received the B.E. degree in surveying and mapping engineering from Central South University, Changsha, China, in June 2014, and the Ph.D. degree in astrometry and celestial mechanics from the Shanghai Astronomical Observatory, Chinese Academy of Sciences, Shanghai, China, in September 2020.

As a Research Assistant, he worked in occultation technology applications in the neutral atmosphere and ionosphere. His research interests include remote sensing of the earth and its atmosphere using global navigation satellite systems, and improving observations for ionospheric data assimilation applications.